PERGAMON

International Journal of Heat and Mass Transfer 42 (1999) 1111–1121

International Journal of HEAT and MASS TRANSFER

A numerical investigation of three-dimensional magnetoconvection in rectangular cavities

Ralph Mößner, Ulrich Müller*

Research Centre of Karlsruhe, Institute of Applied Thermo- and Fluid-dynamics, P.O. Box 3640, D-76021 Karlsruhe, Germany

Received 6 May 1997; in final form 10 September 1997

Abstract

In this paper the influence of stationary magnetic fields of arbitrary direction on three-dimensional natural convection in liquid metals is investigated. The liquid metal is confined in electrically insulating rectangular cavities. The convection is driven by horizontal or vertical temperature gradients. A second-order finite-difference method is employed to solve the basic dimensionless equations. Electric current paths and the effect of resulting Lorentz forces on the organisation of flow and heat transport are studied. Electric currents often close within the fluid without short circuiting through Hartmann layers. Typical flow patterns show excessive intensities in regions close to corners.

Nomenclature

a distance between hot and cold wall
$\mathbf{B}$ magnetic induction
B_0 norm of the external magnetic field
$\mathbf{g}$ acceleration of gravity
h height of the cavity
$\mathbf{j}$ current density
$\mathbf{k}$ unit vector in direction of gravity
$\mathbf{n}$ unit vector normal to the wall
q heat flux density
Q convergence criteria
t time
T temperature
p pressure
$\mathbf{v}$ velocity
v_0 buoyancy velocity
x, y, z non-dimensional coordinates.

Greek symbols

α wave number
β coefficient of thermal expansion
ΔT characteristic temperature difference
Δt timestep
$\Delta x, \Delta y, \Delta z$ non-dimensional grid spacings
η dynamic viscosity
κ thermal diffusivity
λ thermal conductivity
λ_c wavelength of convection rolls
ν kinematic viscosity
ρ density
σ electric conductivity
Φ electric potential.

Non-dimensional parameters

Ha Hartmann number $aB_0\sqrt{\sigma/\eta}$
Nu Nusselt number, $qa/\lambda\Delta T$
Pr Prandtl number, ν/κ
Ra Rayleigh number, $g\beta\Delta T a^3/\mu\kappa$.

1. Introduction

Magnetoconvection plays an important role in geo- and astro-physics. In the outer layers of the Sun and in the Earth's core we find a convective motion which is capable of generating magnetic fields. Related phenomena are investigated in the dynamo theories. Recently,

* Corresponding author. Fax: 0049 07247 82 4837; E-mail: ulrich.mueller@iatf.fzk.de

0017–9310/98 $19.00
PII: S0017–9310(98)00115–X

magnetoconvection became more and more relevant in material processing facilities. The control of crystal growth with the help of external magnetic fields seems to be promising. Therefore, current research has intensified in the field of magnetoconvection and several new results were presented in the last few years. In this context we refer to the publications of Alboussiere et al. [1], Davoust et al. [2], Garandet et al. [3], Hadid and Henry [4] and Ma and Walker [5]. The fundamental nature of magnetoconvection depends on the ratio of magnetic and thermal diffusivity. In astrophysics this ratio is very small whereas on laboratory scale this ratio becomes very large. In our investigation we concentrate on situations where this ratio becomes very large. Furthermore, we only consider the influence of an externally imposed, stationary magnetic field on natural convection. The influence of the velocity field on the magnetic field is neglected, induced magnetic fields are not taken into account. More information about magnetoconvection can be found in the classical works of Chandrasekhar [6], Gershuni and Zhukhovitskii [7] and Proctor and Weiss [8]. In order to study three-dimensional magnetoconvection numerical calculations can be useful. Therefore, we solve the resulting basic dimensionless equations in Cartesian coordinates numerically with a second order finite-difference method.

We present calculations for two different geometries and physical situations. In a first step we investigate the flow in an electrically insulating cube which is heated and cooled at two opposite side walls. Walls which are neither heated nor cooled are assumed to be adiabatic or perfectly heat conducting and the direction of the magnetic field is arbitrary. The Rayleigh number is fixed at $Ra = 10^6$ and the Prandtl number is assumed as $Pr = 0.054$. There exist two publications of Ozoe and Okada [9, 10], one presenting a numerical analysis and one presenting experimental results, which deal with magnetoconvection in the same geometry. These investigations are limited to adiabatic walls and external magnetic fields oriented parallel to the sides of the cube. The present work is aimed at analysing the closure patterns of the electric currents and the resulting Lorentz forces in order to explain the flow patterns for various thermal boundary conditions and directions of the magnetic field. This was not performed by Ozoe and Okada, even not for the directions of the magnetic field they considered. The Nusselt numbers calculated by Ozoe and Okada are compared to those obtained by our computations.

In a second step we investigate the flow in a rectangular cavity with the aspect ratio 6:3:1. The natural convection is driven by a vertical temperature gradient and the magnetic field is oriented vertically, too. Walls which are neither heated nor cooled are assumed to be adiabatic. We present calculations for Hartmann numbers Ha in the range $0 \leqslant Ha \leqslant 60$ for Rayleigh number $Ra \leqslant 5 \cdot 10^4$ and for the Prandtl number $Pr = 0.05$.

2. Basic dimensionless equations

Neglecting displacement currents, induced magnetic fields, dissipation and Joule heating and using the Boussinesq approximation we obtain the following system of nonlinear, partial differential equations describing magnetoconvective flows. These are the continuity equation, the momentum equations, Ohms law, the conservation of electric charge and the energy equation:

$$\nabla \cdot \mathbf{v} = 0 \tag{1}$$

$$\frac{\partial \mathbf{v}}{\partial t} + (\mathbf{v} \cdot \nabla)\mathbf{v} = -\frac{1}{\rho}\nabla p + \frac{1}{\rho}(\mathbf{j} \times \mathbf{B}) + \nu \Delta \mathbf{v} + \beta T \mathbf{g} \tag{2}$$

$$\mathbf{j} = \sigma(-\nabla \Phi - \mathbf{v} \times \mathbf{B}) \tag{3}$$

$$\nabla \cdot \mathbf{j} = 0 \tag{4}$$

$$\frac{\partial T}{\partial t} + \mathbf{v} \cdot \nabla T = \kappa \Delta T. \tag{5}$$

Using the nondimensionalisation explained in Mößner [11] we find the following set of nondimensional equations:

$$\nabla \cdot \mathbf{v} = 0 \tag{6}$$

$$\frac{\partial \mathbf{v}}{qt} + (\mathbf{v} \cdot \nabla)\mathbf{v} = -Ha^2 \sqrt{\frac{Pr}{Ra}} \nabla p + Ha^2 \sqrt{\frac{Pr}{Ra}} (\mathbf{j} \times \mathbf{B}) + \sqrt{\frac{Pr}{Ra}} \nabla \mathbf{v} + T\mathbf{k} \tag{7}$$

$$\mathbf{j} = -\nabla \Phi + \mathbf{v} \times \mathbf{B} \tag{8}$$

$$\nabla \cdot \mathbf{j} = 0 \tag{9}$$

$$\frac{\partial T}{\partial t} + \mathbf{v} \cdot \nabla T = \frac{1}{\sqrt{Ra\, Pr}} \Delta T. \tag{10}$$

In these equations the time t, the pressure p, the density ρ, the electric current density $\mathbf{j}$, the magnetic field $\mathbf{B}$ and the electric potential Φ are made dimensionless with the reference scales a/v_0, $a\sigma v_0 B_0^2$, $a\sigma B_0^2/v_0$, $\sigma v_0 B_0$, B_0 and $a v_0 B_0$. The velocity $\mathbf{v}$ is scaled by the buoyancy velocity $v_0 = \sqrt{g\beta \Delta T a}$ and the temperature T is related to the typical temperature difference ΔT of the problem. As typical temperature difference the temperature difference between the heated and cooled wall is chosen. The unit vector in direction of gravity is characterized by $\mathbf{k}$. The variable a denotes the distance between the heated and the cooled wall of the cavity, σ the electric conductivity, B_0 the norm of the external magnetic field, g the acceleration of gravity and β the coefficient of thermal expansion. Within the set of dimensionless equations we find three-dimensionless parameters, the Hartmann number Ha, the Rayleigh number Ra and the Prandtl number Pr. They are defined as:

$$Ha = aB_0 \sqrt{\frac{\sigma}{\eta}}, \quad Ra = \frac{\beta \Delta T g a^3}{\nu \kappa}, \quad Pr = \frac{\nu}{\kappa}. \tag{11}$$

The Hartmann number Ha represents the square root of

the ratio of electrodynamic to viscous forces. The meaning of the variables a, B_0 and σ has already been explained in the previous paragraph and η represents the dynamic viscosity of the fluid. The Rayleigh number Ra represents the ratio of buoyant energy release to viscous and thermal energy dissipation. In this context ν denotes the kinematic viscosity and κ the thermal diffusivity. The Prandtl number is commonly explained as the ratio of the time scales for diffusion of momentum and heat.

Additionally we introduce the Nusselt number Nu which is defined as

$$Nu = \frac{qa}{\lambda \Delta T}. \tag{12}$$

The Nusselt number is the ratio of entire heat transport to heat transport by heat conduction. The variable q denotes the heat flux density, ΔT the characteristic temperature gradient and λ the thermal conductivity.

In order to solve the dimensionless equations the following boundary conditions are used. The boundary condition for the velocity is the no slip condition

$$\mathbf{v}|_{\text{wall}} = \mathbf{0}. \tag{13}$$

For temperature we employ the boundary conditions

$$T|_{\text{wall}} = f \quad \text{and} \quad \left.\frac{\partial T}{\partial n}\right|_{\text{wall}} = 0. \tag{14}$$

The first condition is used for heated, cooled and perfectly heat conducting walls where f denotes a space dependent function. The second condition is used for adiabatic walls where n denotes the direction normal to the wall.

The boundary condition for the pressure results according to Peyret and Taylor [12] to

$$\left.\frac{\partial p}{\partial n}\right|_{\text{wall}} = 0. \tag{15}$$

Because of the electrically insulating walls we have the homogeneous Neumann boundary condition

$$\left.\frac{\partial \Phi}{\partial n}\right|_{\text{wall}} = 0 \tag{16}$$

for the electric potential.

In the case of electrically insulating walls the normal component of the electric current vanishes at the wall. The boundary condition for the electric current results to

$$\mathbf{j} \cdot \mathbf{n}|_{\text{wall}} = 0. \tag{17}$$

3. Numerical methods

To solve the system of dimensionless equation a finite-difference method in conservation form is used. The calculations are carried out on an equidistant, rectilinear and rectangular grid. Moreover, a staggered grid is preferred. This means that the scalar quantities such as temperature, pressure and the electric potential and the vector components of velocity, electric current density and magnetic field are located at different positions. While the scalars are located in the centre of a computational cell the vector components are located at the boundary of a cell. The use of such a grid prevents unphysical oscillations of the computed pressure as it is possible for regular grids.

In typical calculations in the geometry of the cube $40 \times 40 \times 40$ grids up to $64 \times 64 \times 64$ grids are used. A $40 \times 40 \times 40$ grid results in a equidistant dimensionless gridspacing of $\Delta x = \Delta y = \Delta z = 0.025$. For $64 \times 64 \times 64$ grids one obtains $\Delta x = \Delta y = \Delta z = 0.015625$. The computations are repeated using a $128 \times 40 \times 40$ grid. The maximum number of points ($=128$) is always used in the direction of the magnetic field. If there are two non-zero components of the magnetic field, 128 points are used in each of those directions, whereas the number of gridpoints in direction of the zero component of the magnetic field is reduced to 25. If all components of magnetic field are non-zero, the calculations are repeated with an $80 \times 80 \times 80$ grid. The numerical solutions show for all grids the same qualitative behaviour and differ quantitatively by less than 5%.

The calculations in the geometry with the aspect ratios 6:3:1 are performed with an $80 \times 40 \times 80$ grid which leads to the dimensionless grid spacings $\Delta x = 0.075$, $\Delta y = 0.025$ and $\Delta z = 0.0375$. This calculations are repeated with an $80 \times 80 \times 80$ grid in order to obtain a better resolution of the direction of the magnetic field. As in the case described above the solutions obtained for the different grids agree well.

The discretization of time is performed by explicit schemes. There are two schemes available. The Euler forward scheme is of first order and uses two time levels. It is useful for stationary calculations. The Adams–Bashforth method is of second order and uses three time levels. This method is preferred for time-dependent calculations. The calculations presented in this article are always performed by both schemes. The numerical results obtained by using separately each scheme agree well. Typical dimensionless time steps vary between $\Delta t = 10^{-3}$ and $\Delta t = 10^{-4}$.

For each time step the quotient

$$Q = \frac{|\varphi^{n+1} - \varphi^n|}{|\varphi^n_{\max}|} \tag{18}$$

is calculated for all dependent variables in all gridpoints. The index $n+1$ denotes a discrete point of time which follows the point of time n after a timestep Δt. If $Q \leqslant 10^{-6}$ is valid for all variables in all gridpoints the solution is interpreted as converged.

The spatial discretization is performed by several schemes. If the absolute values of the mesh Reynolds number are small the central-difference scheme is used. Otherwise the LECUSSO upwinding is employed. The acronym LECUSSO means Locally Exact Consistent Upwind Scheme of Second Order. LECUSSO produces

less numerical diffusion than common second-order upwind schemes. This results in more accurate numerical solutions. Details of LECUSSO are explained in Günther [13].

The calculation of velocity and pressure is performed by the fractional-step method. The resulting Poisson equation is solved with SHAFT3 a fast solver for Helmholtz equations using Fourier transformations. The fractional-step method ensures the discrete mass conservation with computer accuracy. Detailed information concerning the fractional-step method can be found in Kim and Moin [14], SHAFT3 is documented in Flassak and Moussiopoulos [15].

4. Results

4.1. Calculations for a horizontal temperature gradient

In this subsection we show results for natural convection in a cube. The flow is driven by a horizontal temperature gradient. For a complete definition of the problem compare Fig. 1.

First we consider a magnetic field in x-direction and adiabatic walls. For this case electric currents are induced by the vertical convective flow at the hot and the cold wall according to Ohms law. The horizontal flow along the top and the bottom wall does not induce electric currents because here the velocity is parallel to the magnetic field. The electric currents induced near the hot and the cold wall run in opposite direction according to the opposite direction of the velocity. The closing pattern of the electric current is illustrated in Fig. 2(a). Since electric charge has to be conserved the electric current has to short circuit somehow. Thus, the electric currents close in planes $y = \text{const.}$ within the fluid. The walls cannot be entered by the electric currents because they are electrically insulating. An important fact is that, unlike in channel flows with electricity insulating walls, the electric currents do not have to pass Hartmann layers. This is due to the symmetry of the flow. As described above, electric currents of opposite direction are induced in the core region of the flow. This current can easily close in the core region without using Hartmann layers. This closing pattern of the electric currents lead to strong Lorentz forces acting against the vertical flow in the core region. Near the corners of the cavity these Lorentz forces vanish because here the electric currents are redirected next to the electrically insulating walls. This results in the flow pattern of Fig. 2(b) which shows strong velocity jets for the velocity component in y-direction near the corner regions. The damping of the natural convection is very strong for this orientation of the magnetic field. In fact, we will show that this direction of magnetic field is most efficient in influencing the heat transport. In Table 1 we see that the average Nusselt number at the hot wall decreases strongly with increasing Hartmann number. The calculated Nusselt numbers show a reasonable agreement with values obtained by Ozoe and Okada in [9] and [10].

Assuming a magnetic field in y-direction and adiabatic walls one finds a similar behaviour. In this case electric currents are induced from the horizontal flow near the top and the bottom wall. These electric currents close in

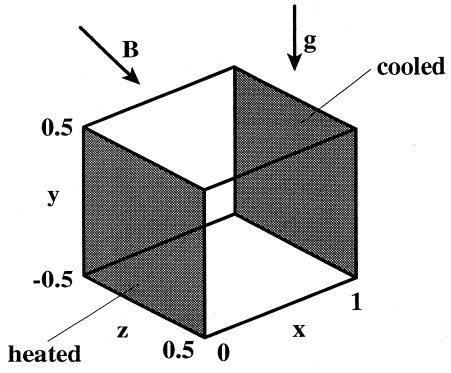

Fig. 1. The investigated physical problem with a horizontal temperature gradient.

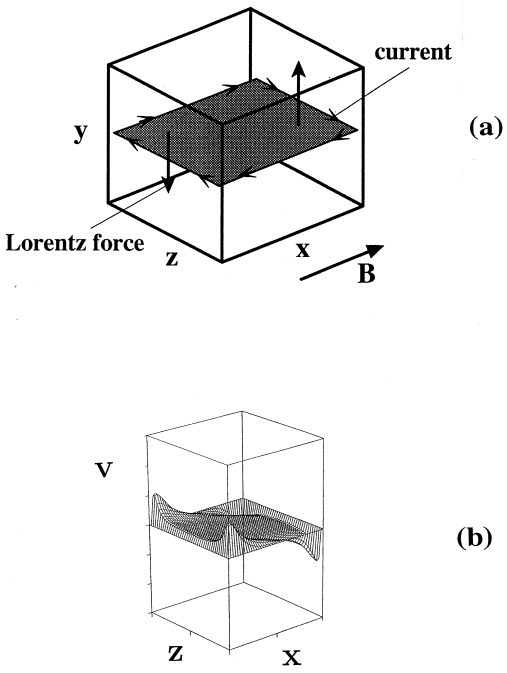

Fig. 2. Results for a magnetic field in x-direction, $Ha = 200$, $Pr = 0.054$ and $Ra = 10^6$: (a) sketch of the closing pattern of the electric current and the resulting Lorentz forces; (b) the velocity in y-direction.

Table 1
Average Nusselt numbers for adiabatic and perfectly heat conducting walls. The magnetic field is oriented in x-, y- or z-direction

	Ozoe/Okada $\overline{Nu}$ for B_x	Mößner $\overline{Nu}$ for B_x	$\overline{Nu}$ for B_y	$\overline{Nu}$ for B_z
	$Pr = 0.054$, $Ra = 10^6$, adiabatic walls			
$Ha = 0$	5.737	7.2	7.2	7.2
$Ha = 100$	4.458	4.766	6.002	7.135
$Ha = 200$	2.917	2.989	4.553	7.050
$Ha = 300$	2.251	2.245	3.475	6.923
	$Pr = 0.054$, $Ra = 10^6$, perfectly conducting walls			
$Ha = 200$	—	1.646	2.224	6.545

planes $x = \text{const.}$ in the core region of the flow and produce Lorentz forces acting against the horizontal flow. As in the case of a magnetic field in x-direction the Hartmann layers become unimportant. According to the same mechanism described in the previous section velocity jets are established in regions near the corners. The difference to the previous situation is that these jets are established for the velocity component in x-direction. The closing pattern of the electric current and the resulting Lorentz forces are displayed in Fig. 3(a). The resulting flow pattern is presented in Fig. 3(b). The electromagnetic damping of the flow is still strong but weaker compared to the arrangement of a magnetic field in x-direction. This can be seen in Table 1.

Considering a magnetic field in z-direction and adiabatic walls the physical situation changes. In a range roughly defined by $0.2 < x < 0.8$ electric currents in negative y-direction are induced by the horizontal flow near the top wall. On the other hand electric currents in positive y-direction are induced near the bottom wall. These currents can only short circuit in planes $x = \text{const.}$ Because the electric currents induced near the bottom wall are in opposite direction compared to the electric currents induced near the top wall the electric currents have to flow in z-direction at a certain point. To establish a short circuit the electric currents have to return in y-direction. This is impossible in the core region because here we have the induced currents coming from the top or bottom wall. The only way to establish a short circuit is to use the Hartmann layers at the walls $z = -0.5$ and $z = 0.5$. This results in an eight-cell-structure which is shown in Fig. 4(a). It has been observed for different

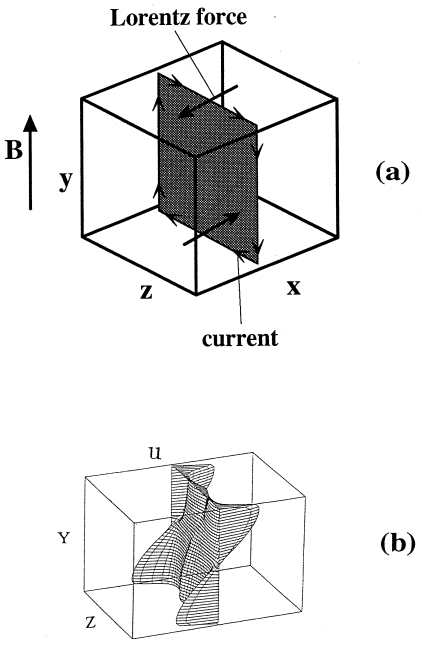

Fig. 3. Results for a magnetic field in y-direction, $Ha = 200$, $Pr = 0.054$ and $Ra = 10^6$: (a) sketch of the closing pattern of the electric current and the resulting Lorentz forces; (b) the velocity in x-direction.

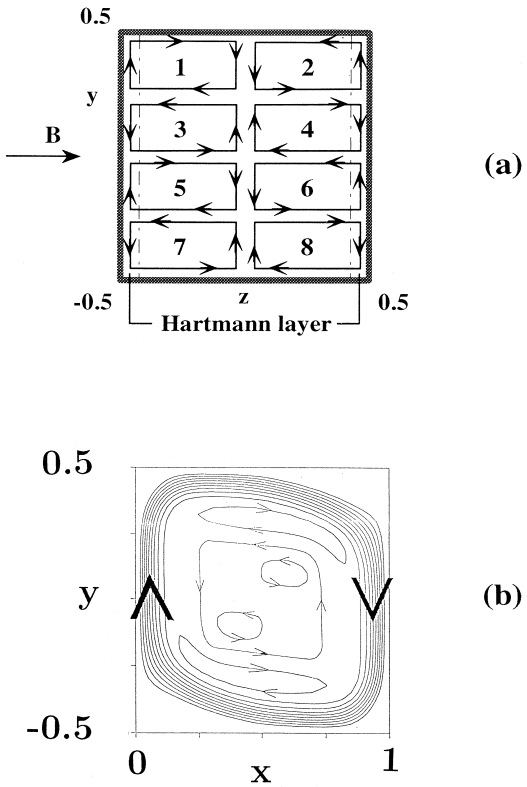

Fig. 4. Results for a magnetic field in z-direction, $Ha = 200$, $Pr = 0.054$ and $Ra = 10^6$: (a) sketch of the closing pattern of the electric current in a plane $x = \text{const.}$ in the region $0.2 < x < 0.8$; (b) streamlines in a plane $z = \text{const.}$

parameter constellations that occasionally a four-cell-structure occurs as possible closing pattern for the electric current. Obviously, we are facing some kind of bifurcation problem. The eight-cell-structure as closing pattern for the electric current has a surprising influence on the flow behaviour. In the inner region of the cube a vortex is generated which rotates in opposite direction compared to the basic vortex which originates from natural convection. This behaviour is illustrated in Fig. 4(b). The electromagnetic damping of the flow is weak because the currents are weak. This in turn is the case because the electric currents have to pass through the high resistivity Hartmann layers. In fact, the average Nusselt number is nearly constant with growing Hartmann numbers in the range $0 \leqslant Ha \leqslant 300$. This is shown in Table 1.

Considering Table 1 it is obvious that the Nusselt number for natural convection which is not influenced by a magnetic field does not agree with the Nusselt number obtained by Ozoe and Okada for the same case. Furthermore, Ozoe and Okada observe a steady state solution while our calculations show a weakly time depended solution. A reason for this could be that in our calculations explicit schemes are used which are underdiffusive. This means that the numerical algorithm damps oscillations not strong enough. On the other hand, Ozoe and Okada use a semi-implicit scheme which is known to produce numerical diffusion and therefore, introducs too much artificial damping. Moreover, we use the LECUSSO upwind scheme which produces much less numerical diffusion than the upwind scheme of first order used by Ozoe and Okada. Because of the high accuracy of the LECUSSO scheme we believe that our numerical results describe the physical phenomena at least semi-quantitatively correct. We have no doubt that the Nusselt numbers obtained in the parameter range $100 \leqslant Ha \leqslant 300$ are quite accurate. For the case $Ha = 0$, we assume that the Nusselt number resulting from our calculation is slightly too large. The Nusselt number obtained by Ozoe and Okada is assumed to be too small, because in the case of a magnetic field in y-direction we find for a Hartmann number of $Ha = 100$ a corresponding Nusselt number of $\overline{Nu} = 6.002$ which is even larger than the Nusselt number obtained by Ozoe and Okada without magnetic field. Therefore, we believe that our calculations are numerically more accurate than the results of Ozoe and Okada.

Although electrically insulating walls normally coincide with adiabatic walls we maintain the electric boundary condition but change the thermal boundary condition from adiabatic to perfectly heat conducting. In this case the fundamental electrodynamic mechanisms described in the previous sections are still observed. The qualitative behaviour of the electric currents and the velocity profiles are unchanged. On the other hand the velocity and therefore the electric current change quantitatively. In addition to this the temperature profiles are changed and as a result the heat transport. Using perfectly heat conducting walls the heat transport is reduced and the average Nusselt number at the hot wall decreases. Considering magnetic fields in x- or y-direction the Nusselt numbers decrease to about half of their values for adiabatic walls. Considering a magnetic field in z-direction one finds a weak decrease of the Nusselt number. The characteristic behaviour of the Nusselt number can be seen in Table 1.

Next, we consider the case of adiabatic walls and assume that, both, a component of the magnetic field in x-direction and a component in y-direction exist. Naturally, the behaviour of the electric current is changed. The vertical and the horizontal flow induce electric currents. The vertical flow induces currents at the hot and the cold wall and the horizontal flow induces currents at the top and bottom wall. The electric currents induced near the hot wall have opposite direction compared to those induced near the top wall. Furthermore, the electric currents induced near the cold wall run in opposite direction compared to those induced near the bottom wall. This leads to a diagonal closing structure of the electric currents. As in the case where the magnetic field is oriented in x- or y-direction only, the electric currents close in the core region of the fluid. Hartmann layers are not important. For reasons already outlined before velocity jets are established in regions near the corners, but here, both, the velocity component in x-direction and in y-direction show this jet like behaviour because there exist strong Lorentz forces acting in x- and y-direction. The diagonal closing structure of the electric currents and the resulting Lorentz forces are illustrated in Fig. 5.

Finally, maintaining the parameter set of the previous paragraph we add a component of the magnetic field in z-direction. If the magnetic field vector is oriented in direction of one space diagonal of the cube all components of the magnetic field have the same size. For this case the diagonal structure of the electric current

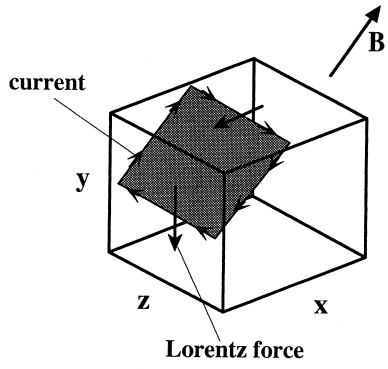

Fig. 5. The closing pattern of the electric current and the resulting Lorentz forces in the case $B_x = 0.707$, $B_y = 0.707$, $B_z = 0$.

described in the previous paragraph can be found once more, however, this structure is changed near the corners. The vertical flow induces together with the z-component of the magnetic field currents in x-direction. Additionally the horizontal flow induces currents in y-direction. These currents close along paths near the corners. This behaviour of the electric current leads to a new structure of the velocity profile. Because of the currents induced by the z-component of the magnetic field the electromagnetic damping of the vertical vanishes at one side. This results in a velocity profile with a jet like behaviour at this particular side. The closing pattern for the electric current and the resulting Lorentz forces are illustrated in Fig. 6(a). The velocity component in y-direction is shown in Fig. 6(b).

If the magnetic field is oriented arbitrarily the behaviour of the electric current and the velocity cannot be predicted exactly. Symmetric flows will not occur. However, experience shows that it is possible to correlate the features of the flow to those investigated before. If one or two components of the magnetic field dominate over the other components the flow behaves nearly like a flow under the influence of a magnetic field where these minor components vanish but non-symmetric effects can be identified.

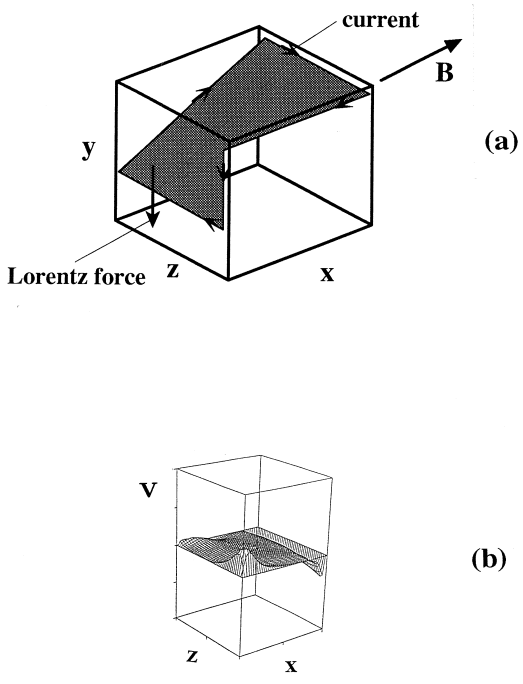

Fig. 6. Results for a magnetic field with the components $B_x = B_y = B_z = 0.577$, for $Ha = 200$, $Pr = 0.054$ and $Ra = 10^6$: (a) the closing pattern of the electric current and the resulting Lorentz forces: (b) the velocity in y-direction.

4.2. Calculations for a vertical temperature gradient

Natural convection driven by vertical temperature gradients is still a challenge for numerical computations. When starting for initial conditions the time to develop stationary flows can be quite large. At high supercritical Rayleigh numbers the flows may even have time periodic and/or chaotic behaviour. Moreover, the damping effect of the magnetic field can lead to delayed restructuring processes in the flow. For numerical computations this leads to extremely large numbers of time steps.

In order to keep the number of gridpoints and thereby the computational time in acceptable limits the computations are limited to rectangular cavities with moderate ratio between longest and shortest side length. Computations are facilitated if the magnetic field vector is parallel to the shortest side wall of the cavity. In this case it is possible to resolve the thin Hartmann boundary layers. The Hartmann layers which occur at walls perpendicular to the magnetic field vector are known to scale with $1/Ha$. Therefore, it is obvious that we need a huge number of gridpoints if the magnetic field vector is oriented parallel to a long side of the cavity using an equidistant grid.

In this subsection we investigate natural convection in a liquid metal with the Prandtl number $Pr = 0.05$ confined in an electrically insulating cavity as shown in Fig. 7. The cavity side lengths ratio is 6 : 3 : 1. The magnetic field vector is parallel to the vector of gravity. The bottom of the container is heated while the top is cooled. The side walls are assumed to be adiabatic.

Before discussing natural convection under the influence of a magnetic field it is useful to describe the fundamental features of the flow without magnetic field. The critical Rayleigh number can be estimated with the help of calculations performed by Kirchartz [16]. We obtain $Ra_{crit} \approx 1950$. For a Rayleigh number slightly above Ra_{crit} we have a stationary flow pattern consisting of six convection rolls. For convective flows in low Prandtl number liquids this six roll solution becomes unstable if the Rayleigh number is slightly increased. We first observe a pulsation of the rolls settling in the long term to trans-

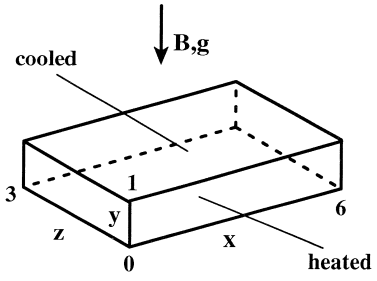

Fig. 7. The investigated physical problem with a vertical temperature gradient.

versally oscillating flow pattern. A detailed description of this flow can be found in Mößner [11]. Increasing the Rayleigh number to values $Ra \geqslant 10^4$ the number of convection rolls decreases to four and the flow is irregularly time-dependent.

The most obvious feature of the magnetoconvective flows is that the number of the rolls depends, in addition to the Rayleigh, also on the Hartmann number. An increase in the Hartmann number leads to an increase of the number of the rolls. The lateral extension of the rolls in the x-direction decreases with increasing Hartmann number. This behaviour is outlined in Table 2. For example, without a magnetic field and for $Ra = 5 \cdot 10^4$ we find four rolls. Calculations for a Hartmann number of $Ha = 30$ result in a six roll pattern. Increasing the Hartmann number to $Ha = 50$ leads to ten rolls. The Hartmann number $Ha = 60$ generates even twelve rolls. The same phenomenon can be observed for the Rayleigh numbers $Ra = 1.5 \cdot 10^4$ and $Ra = 3 \cdot 10^4$. This behaviour of the flow is not surprising as it has been predicted by Chandrasekhar [6] and Gershuni and Zhukhovitskii [7] for the infinite horizontal fluid layer subjected to a vertical magnetic field. According to their theory the width of a convective roll varies as $Ha^{-1/3}$. Furthermore, our calculations show that the number of rolls decrease when the Rayleigh number increases. This effect has frequently been observed without external magnetic field among others by Koschmieder [17] and by Stork and Müller [18] experimentally and by Kirchartz [16] numerically. At a fixed Rayleigh number $Ra = 1.5 \cdot 10^4$ eight rolls occur when a Hartmann number of $Ha = 28$ is used. But when we increase the Rayleigh number to $Ra = 3 \cdot 10^4$ we only find six convection rolls at a Hartmann number of $Ha = 30$. This observation suggests that there is a kind of competition between the buoyancy effects represented by the Rayleigh number and the electromagnetic effects accounted for by the Hartmann number.

Table 2
The average Nusselt number $\overline{Nu}$ and the corresponding flow pattern

Magnetoconvection in a 6 : 3 : 1 cavity Vertical temperature gradient, $Pr = 0.05$, $\mathbf{B} \| \mathbf{g}$		
	$\overline{Nu}$	Flow pattern
$Ra = 1.5 \cdot 10^4$		
$Ha = 0$	1.98	4 rolls, time-dependent
$Ha = 20$	1.32	6 rolls, stationary
$Ha = 25$	1.23	6 rolls, stationary
$Ha = 28$	1.12	8 rolls, stationary
Quadratic extrapolation of our results: $Ha \geqslant 30 \Rightarrow \overline{Nu} = 1$		
Theory for the infinite horizontal fluid layer: $Ha \geqslant 32 \Rightarrow \overline{Nu} = 1$		
$Ra = 3 \cdot 10^4$		
$Ha = 0$	2.49	4 rolls, time-dependent
$Ha = 20$	2.19	6 rolls, stationary
$Ha = 30$	1.57	6 rolls, stationary
$Ha = 35$	1.31	8 rolls, stationary
Quadratic extrapolation of our results: $Ha \geqslant 42 \Rightarrow \overline{Nu} = 1$		
Theory for the infinite horizontal fluid layer: $Ha \geqslant 45 \Rightarrow \overline{Nu} = 1$		
$Ra = 5 \cdot 10^4$		
$Ha = 0$	2.92	4 rolls, time-dependent
$Ha = 30$	2.25	6 rolls, stationary
$Ha = 50$	1.33	10 rolls, stationary
$Ha = 60$	1.16	12 rolls, stationary
$Ha = 60$	1.16	12 rolls, stationary
Quadratic extrapolation of our results: $Ha \geqslant 65 \Rightarrow \overline{Nu} = 1$		
Theory for the infinite horizontal fluid layer: $Ha \geqslant 65 \Rightarrow \overline{Nu} = 1$		

Indeed, the damping effect of the external magnetic field on a natural convection is significant. In Table 2 we can see, that the Nusselt number decreases strongly with increasing Hartmann numbers. As the Nusselt number describes the intensity of the convective heat transport this observation indicates clearly the significant inhibition of the convective heat transfer by the vertical magnetic field. At a Rayleigh number of $Ra = 1.5 \cdot 10^4$ the Nusselt number is about 43% smaller for the case $Ha = 28$ compared to the $Ha = 0$. For a Rayleigh number of $Ra = 3 \cdot 10^4$ a Hartmann number of $Ha = 30$ reduces the Nusselt number by about 37% compared to the case $Ha = 0$. And even for a Rayleigh number of $Ra = 5 \cdot 10^4$ the Nusselt number in the case $Ha = 30$ is about 23% smaller than the Nusselt number obtained for $Ha = 0$.

Comparing the critical parameters (Ra_c, Ha_c) for which natural convection is entirely suppressed with equivalent parameter values for an infinite horizontal fluid layer we find good agreement. The average Nusselt number satisfies the condition $\overline{Nu} = 1$ if the natural convection is totally damped. At a Rayleigh number of $Ra = 1.5 \cdot 10^4$ the Nusselt number is $\overline{Nu} = 1.12$ for $Ha = 28$ as we can see in Table 2. The critical Hartmann number Ha for which the Nusselt number takes the value $\overline{Nu} = 1$ can be estimated by a quadratic extrapolation of our results obtained for Hartmann numbers $Ha = 20$, 25, 28 to $Ha = 30$. The theory for the infinite horizontal fluid layer presented by Chandrasekhar [6] predicts a value of $Ha = 32$ in this case. This demonstrates a reasonable agreement, taking into account that the side walls of the cavity introduce an additional viscous damping effect on the convection. For Rayleigh numbers $Ra = 3 \cdot 10^4$ and $Ra = 5 \cdot 10^4$ we obtain corresponding results.

It is striking that we only find stationary solutions for the considered parameter range. Higher order instabilities and time-dependent flows reported by Clever and Busse [19] for the equivalent problem of an infinite horizontal fluid layer cannot be observed. We conjecture that the Hartmann numbers considered in our computations are large enough to suppress time-dependent solutions.

A stability diagram of Clever and Busse [19], presented in Fig. 8, supports this conjecture. In this diagram the region of stable stationary solutions and the regions of several instabilities are shown in dependence of the Rayleigh number and the wave number α. The wave number α is defined as $\alpha = 2\pi h/\lambda_c$, where h represents the height of the container while λ_c denotes the wave length of the convection rolls. Inserting one of our results obtained for the parameters $Ha = 20$ and $Ra = 1.5 \cdot 10^4$ into this diagram, we find that our result is located in a region where stationary two-dimensional roll patterns are stable. However, this comparison has to be taken with some caution since there are some slight differences in the parameters. The diagram of Busse and Clever shows results for $Ha = 22$ and $Pr = 0.01$ while our calculation is performed for $Ha = 20$ and $Pr = 0.05$. Moreover, we consider a container of finite length compared to an infinite horizontal fluid layer investigated by Clever and Busse. It is impossible to compare further results of our computations with the stability diagram of Clever and Busse because our values for the Hartmann number or the Rayleigh number differ too much compared to those of the diagram.

Velocity profiles of the numerical solutions are shown in Figs 9 and 10. We see that the profiles are characterized by jet-like velocity distributions in regions to the corners formed by the horizontal boundaries and the side walls perpendicular to the roll axes. Here, we find strong velocity gradients whereas the velocity is nearly constant along the vortex axes in the core region. This jet character near the corners can be found for the horizontal and the vertical velocity component as one can see in Figs 9 and 10.

The velocity distribution is easily explained by analysing the paths of the electric currents and the resulting Lorentz forces. The only conceivable and consistent closure pattern for the electric currents is sketched in Fig. 11 together with the related double roll flow pattern. In principle any fluid motion in x-direction induces electric

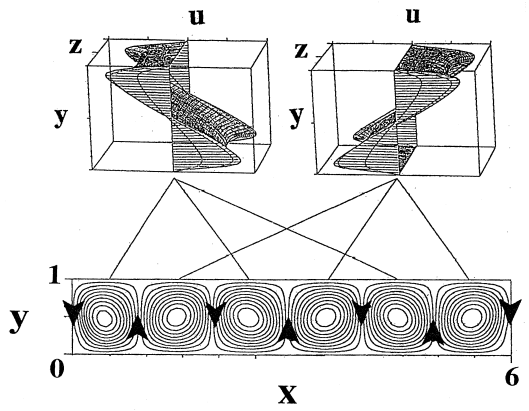

Fig. 9. The horizontal velocity component and the projected streamline pattern in a plane $z = \text{const.}$ for $Ra = 3 \cdot 10^4$, $Ha = 30$ and $Pr = 0.05$.

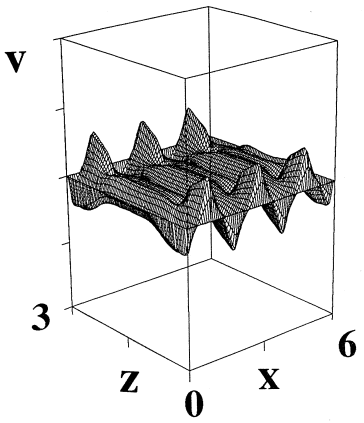

Fig. 10. The vertical velocity component for $Ra = 3 \cdot 10^4$, $Ha = 30$ and $Pr = 0.05$. The geometry is presented distortly to show the jet like behaviour more clearly.

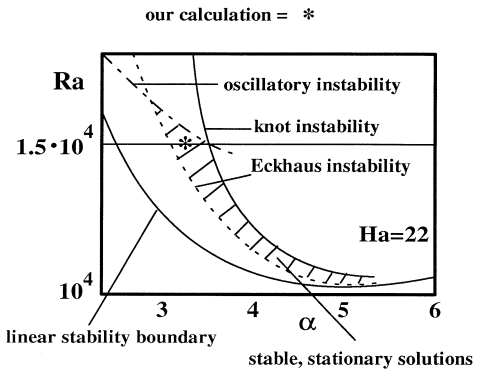

Fig. 8. Integration of one of our results in a stability diagram of Clever and Busse [19].

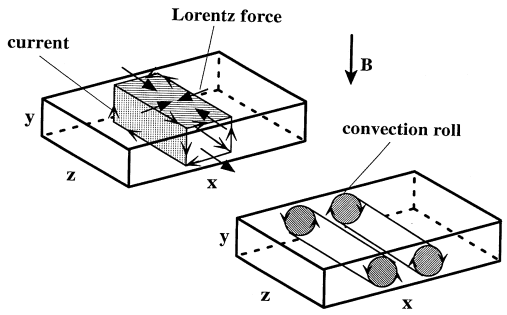

Fig. 11. Sketch of the closing pattern of the electric current and the corresponding flow pattern of neighbouring roll cells.

currents in z-direction according to the vertical B-field and Ohms law. Vertical motion, however, does not affect the current distribution. The currents have to short circuit within the conducting fluid, since the confining walls were assumed to be electrically insulating. In each convection roll currents which are induced near the bottom plate run in the opposite direction to those induced near the top plate. Moreover, in two adjacent parallel rolls the electric currents which are induced near the bottom or top boundary are opposite to each other as the horizontal components of velocity have opposite direction. Because of the charge conservation requirement the electric currents have to short circuit.

Moreover, as indicated in Fig. 11, the induced electric currents give rise to Lorentz forces which counteract the buoyancy induced horizontal flow in each roll in the core region. Thereby, a significant braking effect on the convection rolls is generated. This braking effect is absent near the side walls perpendicular to the roll axes. Here, Lorentz forces vanish because electric currents run parallel to the magnetic field or Lorentz forces are parallel to the roll axes. In the second case the Lorentz forces point in opposite direction near the bottom or top plate and the direction of the forces is reversed in a neighbouring convection roll. The missing or at least reduced braking effect results in a jet like velocity distribution in each roll near the side walls. This explains the observations presented in Figs 9 and 10.

5. Summary and conclusions

This paper presents numerical solutions for natural convection of a liquid metal confined in electrically insulating rectangular cavities. The flow is subjected to an external stationary magnetic field. For a horizontal temperature gradient a magnetic field perpendicular to the heated wall is most effective in damping the natural convection. A horizontal magnetic field parallel to the heated side wall results in the least damping. In the case of vertical temperature gradient the number of convection rolls depends on the Rayleigh and the Hartmann number. Increasing Rayleigh numbers decrease and increasing Hartmann numbers increase the number of convection rolls in the cavity. The resulting Lorentz forces and their braking effect explain the seemingly strange shape of the velocity profiles with excessive intensities in regions near the corners.

Thus, as in common MHD-flows, the paths of the induced electric currents and the resulting Lorentz forces govern the particular phenomena of magnetoconvection. Often electric currents short circuit in the core region of the flow without passing Hartmann layers, therefore the resulting damping of the flow is quite strong. This is a major difference to MHD channel flows where electrically insulating walls lead to a weak damping of the flow. This result is in good agreement with the findings of Davoust et al. [2].

Acknowledgements

This article contains the essential results of the Ph.D. thesis of R. Moessner. The work was performed within the Project Fusion Technology of the Research Centre Karlsruhe. R. Moessner acknowledges the grant of a Ph.D. scholarship by the Forschungszentrum.

References

[1] T. Alboussiere, J. Garandet, R. Moreau, Buoyancy-driven convection with a uniform magnetic field, part 1, asymptotic analysis, Journal of Fluid Mechanics 253 (1983) 545–563.
[2] L. Davoust, R. Moreau, R. Bolcato, Influence of a vertical magnetic field on convection in the horizontal Bridgmann crystal growth configuration, Second International Conference on Energy Transfer in Magnetohydrodynamic Flows PAMIR 1 (1994) 47–56.
[3] J. Garandet, T. Alboussiere, R. Moreau, Buoyancy-driven convection in a rectangular enclosure with a transverse magnetic field, International Journal of Heat and Mass Transfer 35 (1992) 741–748.
[4] H. Hadid, D. Henri, Numerical simulation of convective three-dimensional flows in a horizontal Bridgeman configuration under the action of a constant magnetic field, Second International Conference on Energy Transfer in Magnetohydrodynamic Flows, PAMIR 1 (1994) 47–56.
[5] N. Ma, J. Walker, Liquid–metal buoyant convection in a vertical cylinder with a strong vertical magnetic field and with nonaxisymmetric temperature, Physics of Fluids 7 (8) (1995) 2061–2071.
[6] S. Chandrasekhar, Hydrodynamic and Hydromagnetic Stability, Dover Publications, New York, 1961.
[7] G. Gershuni, E. Zhukhovitskii, Convective Stability of Incompressible Fluids, Verlag Nauka, Moscow, 1972.
[8] M. Proctor, N. Weiss, Magnetoconvection, Reports of Progress in Physics 45 (1982) 1317–1379.
[9] H. Ozoe, K. Okada, The effect of the direction of the external magnetic field on the three-dimensional natural convection in a cubical enclosure, International Journal of Heat and Mass Transfer 32 (1989) 1939–1954.
[10] H. Ozoe, K. Okada, Experimental heat transfer rates of natural convection of molten gallium suppressed under an external magnetic field in either the x, y, or z direction, Journal of Heat Transfer 114 (1992) 107–114.
[11] R. Mößner, Dreidimensionale numerische Simulation von Naturkonvektions-strömungen unter dem Einfluß von Magnetfeldern, Bericht des Forschungszentrums Karlsruhe, FZKA 5748, 1996.
[12] R. Peyret, T. Taylor, Computational Methods of Fluid Flow, Springer-Verlag, New York, 1983.
[13] C. Günther, Conservative versions of the locally exact con-

sistent upwind scheme of second order (LECUSSO-Scheme), International Journal of Numerical Methods in Engineering 34 (1992) 793–804.

[14] J. Kim, P. Moin, Application of a fractional-step-method to incompressible Navier–Stokes equations, Computational Fluid Dynamics Branch, NASA Ames Research Center, Moffett Field, CA, 1984.

[15] T. Flassak, N. Moussiopoulos, A fully vectorised fast direct solver of the Helmholtz equation, Proceedings of the first international conference in supercomputing in Southampton, U.K. 1989, pp. 67–77.

[16] K. Kirchartz, Dreidimensionale Konvektion in quaderförmigen Behältern, von der Fakultät für Machinenbau der Universität karlsruhe genehmigte Habilitations-schrift, 1988.

[17] E. Koschmieder, On the wavelength of convective motions, Journal of Fluid Mechanics 35 (1969) 527–530.

[18] K. Stork, U. Müller, Convection in boxes: experiments, Journal of Fluid Mechanics 54 (1972) 599–611.

[19] R. Clever, F. Busse, Three-dimensional convection in the presence of strong vertical magnetic fields, Eur. J. Mech., B/Fluids 15 (1996) 1–15.